Shi, P., Wei, M., and Pockalny, R.A., 2021, The ubiquitous creeping segments on oceanic transform faults: Geology, https://doi.org/10.1130/G49562.1

Supplementary Material for

The Ubiquitous Creeping Segments on Oceanic Transform Faults

Pengcheng Shi[1], Meng (Matt) Wei[1], Robert A. Pockalny[1]

[1]*Graduate School of Oceanography, University of Rhode Island, Narragansett, RI, 02882, USA*

This supplementary material aims to provide further details for the DATA & METHODS section in the main context.

DATA & METHODS

Surface Wave Cross-correlation

For each oceanic transform fault (OTF), we manually defined a search box (Table S1) encompassing it and expanded it by 0.5 degree both in latitude and longitude to account for the initial location mismatch in the USGS catalogs. The lower cutoff magnitude in our analysis is Mw 5.0 on 104 faults but is larger on faults that generate M≥6.2 earthquakes (Table S1).

Two events are formed as a pair for further cosine fitting only if (1) the initial USGS catalog location difference is within 125 km, and (2) both moment magnitudes are above 6.0, or their difference is below 0.4. A valid differential time requires its cross-correlation coefficient above 0.70 and itself below 35 seconds to reduce the number of obvious outliers. A valid cosine fitting requires at least eight differential time, and the azimuthal gap is no larger than 120 degrees. In the cosine fitting, we used soft-L1 loss which combines the smoothness of L2 norm and the robustness to outliers of L1 norm (Shearer, 1997). Each fitted cosine curve gives the catalogue time shift t_r, the relative distance d_r and the azimuth θ_r. Uncertainties of each parameter (δt_r, δd_r, $\delta\theta_r$) are computed via the bootstrap method (Wolfson-Schwehr et al., 2014), however, instead of using one second, we used the differential time residual with respect to our best fit as the standard error for bootstrapping.

Optimization of the Event Cluster's Location

In order to perform relative relocation, we approached as following. Of each fault, we use, for instance NetworkX (Hagberg et al., 2008), to build a graph $G = G(V, E)$, where vertices $V = V(\text{lat}, \text{lon})$ denote each event's geodetic coordinate and edges $E = E(d_r, \theta_r, \delta d_r, \delta\theta_r)$ whenever the two event has meaningful relative location information from the previous cosine fitting. We used breadth first search (BFS) to identify isolated event clusters and performing one-way relocation using d_r and θ_r, in such case, each group was relocated using the latest event as reference. This can largely correct obviously erroneous locations originally from the catalogue as well as serve as appropriate initial conditions for later optimization. Then, we traversed (BFS) through each vertex V_i and updated their location in-place by minimizing:

$$L(V_i) = \sum_{\substack{e \in E_i \\ V_j \in e,\, V_i \neq V_j}} \left| \frac{D(V_i, V_j) - d_r^{ij}}{\delta d_r^{ij}} \right| + \lambda \left| \frac{\Theta(V_i, V_j) - \theta_r^{ij}}{\delta \theta_r^{ij}} \right| \quad (1)$$

Here E_i denotes all edges connected to V_i, V_j all vertices connected to V_i. D and Θ are the function computing distance and azimuth given two geodetic location, for instance by using PROJ (PROJ contributors, 2020). λ is a hyperparameter and we simply chose 1 as the distance ranges approximately from 0 to 125 km and the azimuth from 0 to 180 degrees, whose numerical scales are similar to each other. We minimized the residual of containing relative distance as well as azimuth both weighted by their uncertainties respectively. Nelder-Mead method was applied here since it is robust in many cases where derivative cannot be readily evaluated (Nelder and Mead, 1965; Wright, 1996; Virtanen et al., 2020). This is different from HypoDD algorithm (Waldhauser and Ellsworth, 2000) in which they linearized travel time difference with respect to spatial coordinates.

At last, to incorporate potential cyclic constraints (e.g., more than 2 events are mutually correlated) in the graph and for a finer tuning, we put all the information together to update location by minimizing:

$$L(V) = \sum_{V_i \in V} L(V_i) \tag{2}$$

Here we bounded λ between 0.2 to 2.0. We simply used local derivative-free method such as COBYLA (Powell, 1994; Johnson, 2020) as we found the last step did not alter the optimization results from the previous step to any significant extent, indicating the optimization probably converged already. So far, we obtained the relocated relative positions within each group of events for each OTF. For the future improvement we can incorporate source correction as highlighted in Howe et al., (2019).

Translation of the Event Cluster's Location

If hydroacoustic catalogs covering the OTFs are available, we selected the latest M5 event as the reference for the associated cluster because of its small location error (mostly < 5 km) and proximity to epi-centroid (Pan and Dziewonski, 2005). Locations of M≥6 events in hydroacoustic catalogs are not accurate due to energy clipping (Fox et al., 2001). In case of no hydroacoustic events for reference, we manually shifted the cluster to match the geological feature if good bathymetry data is available and the earthquakes are clearly offset from the geological features (Pan et al., 2002).

Empirical Subsurface Rupture Length

A comparison between the empirical subsurface rupture length based on Wells and Coppersmith (1994) and observations from two detailed studies is shown in Figure S1. We excluded events with explicit non-strike-slip focal mechanisms (rake angle > 25) when calculating the subsurface rupture length and the average moment release rate curve subsequently. For events without focal mechanisms (mostly before 1995), we assumed them as strike-slip since our data focus on OTFs.

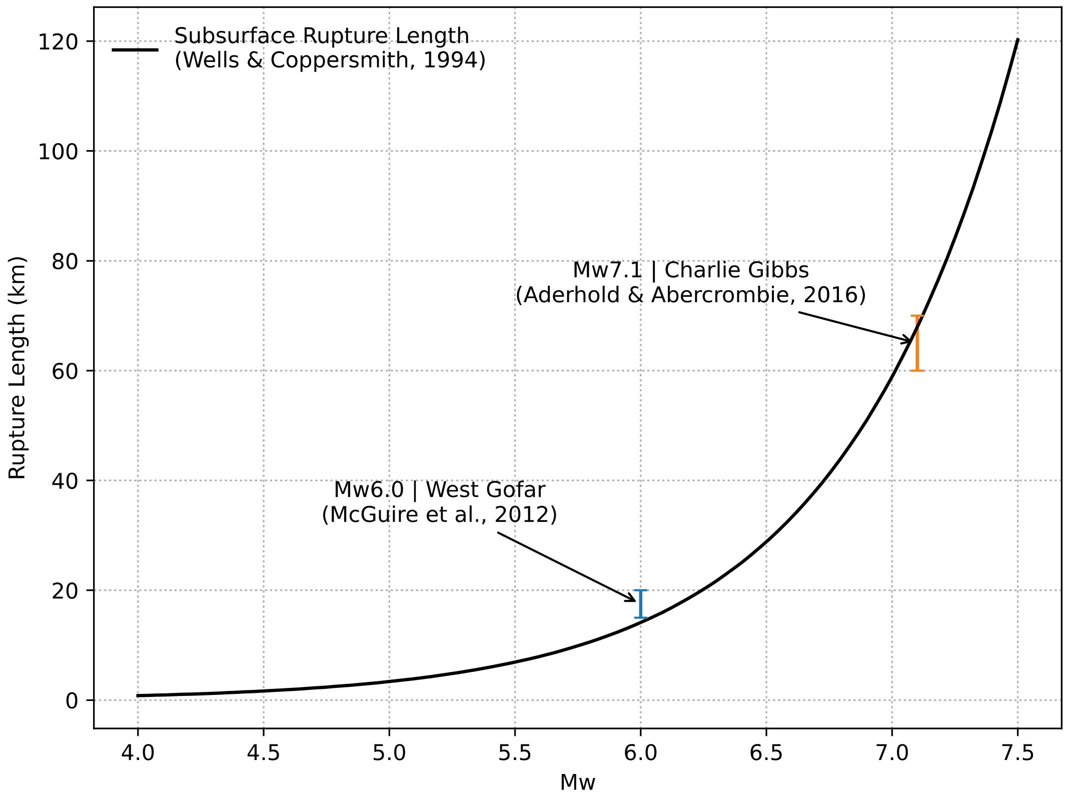

Figure S1. A comparison between the empirical subsurface rupture length and observations from two detailed studies. The solid black line denotes the subsurface rupture length based on Wells and Coppersmith (1994). The blue error bar (15 – 20 km) denotes the rupture length of those periodic Mw 6.0 events on West Gofar OTF. The value is inferred from the afterslip distribution from the 2008 Mw 6.0 event (McGuire et al., 2012). The orange error bar (60 – 70 km) denotes the rupture length of several Mw 7.0 events on Charlie Gibbs OTF recalibrated by Aderhold and Abercrombie, (2016).

TABLE S1. FAULT INFORMATION AND RESULTS

Name	Lat	Lon	Length (km)	Plate Rate (mm/yr)	Min Lat	Max Lat	Min Lon	Max Lon	Mw THLD	GMRT*	Spatial type[†]	CSF[§] (reloc)	CSF[§] (1950)
Aden Ridge													
Alula Fartak	13.90	51.70	203	19.4	13.11	14.85	51.17	52.30	5.4	Bad	GeoStruct	0.51	0.33
Owen	11.50	57.50	335	23.9	10.03	13.01	56.62	58.61	5.2	Bad	FaultProp	0.66	0.36
America Antarctic Ridge													
Bullard (A)	-59.10	-17.20	95	17.2	-59.42	-58.60	-18.40	-16.18	5.0	Bad	FaultProp	0.38	0.13
Bullard (B)	-58.20	-11.90	526	17.5	-58.63	-57.67	-16.06	-6.73	5.6	Bad	FaultProp	0.69	0.59
Conrad	-55.70	-3.30	198	18.5	-55.94	-55.20	-4.82	-1.50	5.3	Bad	GeoStruct	0.57	0.47
South Sandwich	-60.85	-22.88	383	12.3	-61.03	-60.30	-27.02	-18.63	5.0	Medium	FaultProp	0.40	0.30
Central Indian Ridge													
Argo	-13.70	66.30	102	37.6	-14.18	-13.19	65.66	66.83	5.0	Bad	FaultProp	0.65	0.43
CIR 10S	-10.09	66.56	76	31.0	-10.45	-9.81	66.20	66.86	5.0	Bad	FaultProp	0.93	0.88
CIR 12'12	-11.90	65.70	106	35.5	-12.32	-10.85	65.21	67.01	5.0	Bad	FaultProp	0.86	0.74
CIR 16S	-16.29	66.97	110	35.6	-16.59	-16.01	66.50	67.38	5.0	Bad	FaultProp	0.60	0.54
CIR 1S	-1.19	67.52	50	29.9	-1.43	-0.87	67.39	67.82	5.0	Bad	FaultProp	0.49	0.31
CIR 5S	-4.73	68.59	49	31.0	-4.92	-4.52	68.45	68.80	5.0	Bad	FaultProp	0.64	0.64
CIR 6S	-6.83	68.24	89	31.4	-7.19	-6.61	67.88	68.49	5.0	Bad	FaultProp	0.75	0.60
CIR 7S	-7.61	68.08	62	30.2	-7.87	-7.36	67.86	68.33	5.0	Bad	FaultProp	0.74	0.66
Egeria	-20.13	66.58	46	38.1	-20.23	-19.95	66.33	66.76	5.0	Bad	FaultProp	0.68	0.37
Flinders	-20.24	67.26	65	38.5	-20.45	-20.09	66.96	67.50	5.0	Bad	FaultProp	0.83	0.71
Gemino	-22.90	69.20	38	47.3	-23.57	-21.90	68.75	69.93	5.0	Bad	FaultProp	0.69	0.60
Mabahiss	-3.04	68.12	42	30.5	-3.22	-2.81	68.01	68.32	5.0	Bad	Undecided	0.60	0.31
Marie Celeste	-17.40	65.90	219	40.8	-18.15	-16.86	64.85	67.14	5.2	Bad	FaultProp	0.41	0.13
Sealark	-3.88	68.47	63	30.8	-4.08	-3.53	68.33	68.75	5.0	Bad	FaultProp	0.84	0.37
Vema II	-8.90	67.50	237	34.0	-9.82	-8.11	66.38	68.33	5.0	Bad	FaultProp	0.66	0.49
Vityaz	-5.69	68.37	105	31.1	-6.10	-5.22	68.02	68.78	5.0	Bad	FaultProp	0.85	0.74
Chile Rise													
Challenger	-37.11	-95.72	247	44.6	-37.43	-36.86	-97.03	-93.99	5.0	Good	GeoStruct	0.84	0.78
Chile	-35.50	-103.20	1099	58.8	-36.52	-34.22	-110.12	-96.95	5.8	Bad	GeoStruct	0.69	0.56
Chile 38S	-38.33	-93.63	111	46.9	-38.46	-38.18	-94.02	-92.48	5.0	Good	GeoStruct	0.86	0.76
Chile 39S	-38.96	-92.07	84	47.0	-39.13	-38.77	-92.94	-91.26	5.0	Good	FaultProp	0.37	0.32
Chiloe	-43.03	-83.08	61	47.8	-43.31	-42.81	-83.89	-82.55	5.0	Good	FaultProp	0.46	0.38
Darwin	-45.90	-76.37	53	48.3	-46.01	-45.78	-76.74	-76.02	5.0	Medium	FaultProp	0.39	0.26
Guafo	-44.70	-80.15	286	48.1	-45.29	-44.14	-82.37	-78.01	5.6	Medium	FaultProp	0.69	0.51
Guamblin	-45.70	-77.37	80	48.3	-45.84	-45.56	-77.95	-76.89	5.0	Bad	FaultProp	0.36	0.26
Valdivia	-41.50	-88.80	599	60.0	-41.47	-40.87	-91.80	-84.10	5.3	Bad	GeoStruct	0.80	0.56
East Pacific Rise													
Clipperton	10.20	-104.00	84	105.3	10.08	10.30	-104.33	-103.48	5.0	Good	FaultProp	0.41	0.14
Discovery	-4.00	-104.20	63	137.9	-4.07	-3.92	-104.50	-103.80	5.0	Good	GeoStruct	0.38	0.33
Garrett	-13.40	-111.80	124	149.8	-13.61	-13.25	-112.33	-111.16	5.0	Good	FaultProp	0.70	0.47
Goc 24N	24.24	-109.05	124	50.4	24.09	24.49	-109.44	-108.09	5.6	Good	FaultProp	0.65	0.50
Goc 25N	24.98	-109.52	119	49.9	24.40	25.50	-110.07	-108.80	5.6	Good	FaultProp	0.24	0.22
Gofar	-4.50	-105.40	170	138.8	-4.92	-4.26	-106.28	-104.60	5.4	Good	GeoStruct	0.45	0.15
Orozco	15.20	-105.00	89	86.5	15.15	15.56	-105.32	-104.31	5.0	Good	FaultProp	0.85	0.59
Quebrada	-3.80	-103.20	118	137.4	-4.00	-3.40	-104.22	-102.72	5.0	Good	FaultProp	0.76	0.73
Rivera	19.00	-107.40	374	71.2	17.95	19.80	-109.30	-104.95	5.8	Medium	FaultProp	0.77	0.58
Siqueiros	8.40	-103.50	110	111.9	8.20	8.62	-104.20	-102.89	5.0	Good	GeoStruct	0.57	0.46
Tomayo	23.08	-108.34	65	51.0	22.59	23.40	-108.85	-107.84	5.6	Medium	FaultProp	0.65	0.54
Wilkes	-9.00	-109.00	109	145.0	-9.30	-8.70	-110.25	-108.30	5.0	Good	FaultProp	0.53	0.39
Yaquina	-6.20	-107.20	44	141.4	-6.43	-6.13	-107.48	-106.83	5.0	Good	FaultProp	0.77	0.67
Gorda Ridge													
Mendocino	40.37	-126.04	237	49.5	40.14	40.50	-129.79	-124.41	5.6	Good	FaultProp	0.56	0.41
Juan De Fuca													
Blanco	43.80	-128.50	335	59.4	42.78	44.41	-130.45	-125.92	5.4	Medium	GeoStruct	0.61	0.37

Sovanco	49.00	-130.00	135	38.0	48.69	49.41	-130.65	-128.68	5.0	Good	Undecided	N/A	N/A
<u>Mid-Atlantic Ridge</u>													
15'20	15.40	-45.80	193	26.4	14.95	15.50	-46.75	-44.85	5.0	Medium	GeoStruct	0.57	0.61
Ascension	-7.37	-13.25	261	35.0	-7.70	-6.58	-13.97	-11.35	5.2	Medium	FaultProp	0.70	0.51
Atlantis	30.10	-42.40	63	23.6	29.85	30.23	-42.69	-41.72	5.0	Good	FaultProp	0.80	0.52
Bode Verde	-12.25	-14.59	218	30.0	-12.48	-11.36	-15.05	-12.82	5.0	Bad	FaultProp	0.54	0.44
Chain	-1.20	-14.50	313	33.0	-1.61	-0.66	-16.00	-12.90	5.6	Medium	GeoStruct	0.49	0.23
Charlie Gibbs (A)	52.70	-33.40	203	22.4	52.40	53.00	-34.66	-32.35	5.0	Bad	FaultProp	0.59	0.31
Charlie Gibbs (B)	52.20	-30.90	110	15.9	51.90	52.50	-31.58	-29.80	5.0	Bad	FaultProp	0.80	0.76
Doldrums	7.60	-36.90	726	29.3	7.32	7.77	-40.80	-33.53	5.5	Bad	GeoStruct	0.81	0.58
Falkland	-47.20	-11.90	181	33.4	-47.65	-46.83	-13.73	-10.16	5.0	Medium	FaultProp	0.71	0.56
Gough	-39.79	-16.23	56	29.0	-39.97	-39.60	-16.62	-15.81	5.0	Bad	FaultProp	0.90	0.81
Hayes	33.60	-38.60	80	22.6	33.30	33.92	-38.90	-37.44	5.0	Good	FaultProp	0.69	0.72
Jan Mayen	71.30	-9.10	220	17.3	70.90	72.30	-14.00	-7.00	5.0	Bad	FaultProp	0.30	0.11
Kane	23.80	-45.60	146	25.2	23.57	23.86	-46.35	-44.65	5.0	Good	FaultProp	0.53	0.29
MAR 18S	-17.72	-13.37	91	30.3	-17.93	-17.49	-13.75	-12.63	5.0	Bad	FaultProp	0.70	0.46
MAR 21S	-21.23	-11.72	45	30.4	-21.38	-21.10	-12.09	-11.52	5.0	Bad	FaultProp	1.00	0.64
MAR 22S	-22.82	-13.26	193	30.4	-23.03	-21.81	-13.76	-11.73	5.0	Bad	GeoStruct	0.83	0.74
MAR 25 50S	-25.66	-13.74	39	30.3	-25.87	-25.35	-14.03	-12.65	5.0	Good	FaultProp	0.40	0.36
MAR 25S	-24.90	-13.55	37	30.4	-25.02	-24.79	-13.80	-13.40	5.0	Bad	FaultProp	0.53	0.53
MAR 29 45S	-29.76	-13.77	27	30.1	-29.87	-29.63	-14.01	-13.54	5.0	Good	FaultProp	1.00	0.83
MAR 29S	-29.19	-13.45	133	30.1	-29.35	-28.70	-13.86	-12.44	5.0	Bad	GeoStruct	0.81	0.70
MAR 32S	-32.50	-14.42	109	29.9	-32.69	-31.96	-14.82	-13.25	5.0	Good	GeoStruct	0.89	0.62
MAR 34S	-34.16	-14.83	69	29.7	-34.37	-33.96	-15.52	-14.28	5.0	Medium	FaultProp	0.88	0.88
MAR 35S	-35.40	-16.50	250	35.5	-35.66	-35.05	-17.76	-14.77	5.8	Bad	FaultProp	0.55	0.38
MAR 40S	-40.35	-16.64	40	28.9	-40.43	-40.21	-16.89	-16.42	5.0	Bad	FaultProp	0.80	0.58
MAR 50S	-49.13	-9.14	110	26.9	-49.33	-48.84	-9.62	-8.11	5.0	Bad	FaultProp	0.84	0.58
MAR 5S	-5.04	-11.94	78	29.3	-5.10	-4.80	-12.03	-11.28	5.0	Bad	FaultProp	0.98	0.84
Marathon	12.64	-44.46	88	24.4	12.57	12.72	-44.92	-43.77	5.0	Good	FaultProp	0.91	0.79
Oceanographer	35.10	-35.60	121	22.0	35.00	35.36	-36.55	-35.10	5.0	Good	FaultProp	0.37	0.31
Rio Grande	-28.23	-12.94	57	30.2	-28.42	-28.05	-13.30	-12.52	5.0	Medium	FaultProp	0.69	0.64
Romanche	-0.30	-20.60	878	32.5	-1.60	0.80	-24.72	-15.80	5.8	Bad	GeoStruct	0.71	0.49
St Paul	0.60	-27.60	589	31.9	0.15	1.40	-30.45	-24.36	5.5	Bad	GeoStruct	0.68	0.56
Strakhov	3.94	-32.08	108	27.0	3.69	4.12	-32.74	-31.56	5.0	Good	FaultProp	0.69	0.69
Tetyaev	-16.25	-13.75	123	30.3	-16.48	-16.04	-14.43	-13.04	5.0	Bad	FaultProp	0.83	0.82
Vema	10.90	-42.30	307	28.2	10.50	11.00	-43.70	-40.11	5.5	Good	FaultProp	0.61	0.31
<u>Pacific Antarctic Ridge</u>													
Heezen	-55.70	-124.50	382	83.8	-56.50	-54.65	-127.57	-121.51	5.8	Medium	FaultProp	0.67	0.44
Herron	-56.50	-139.20	26	79.7	-56.36	-56.03	-139.83	-138.83	5.0	Medium	FaultProp	0.43	0.42
Hollister	-54.40	-136.10	119	82.5	-54.78	-54.05	-137.00	-135.18	5.5	Medium	FaultProp	0.19	0.13
L'Astronome	-59.65	-150.85	56	68.9	-59.91	-59.35	-151.49	-150.11	5.0	Good	FaultProp	0.24	0.14
Le Geographe	-57.63	-147.50	70	71.9	-57.91	-57.34	-148.07	-146.83	5.0	Medium	FaultProp	0.37	0.36
Menard	-49.60	-115.30	208	90.5	-50.03	-49.14	-116.68	-113.66	5.6	Medium	FaultProp	0.54	0.51
PAR 161	-61.78	161.50	77	46.0	-62.16	-61.46	160.93	161.97	5.0	Bad	FaultProp	0.34	0.18
PAR 163	-62.10	163.36	85	46.7	-62.57	-61.80	162.98	163.95	5.0	Bad	FaultProp	0.88	0.67
PAR 165	-62.38	165.46	89	47.6	-62.75	-61.93	165.04	165.77	5.0	Bad	FaultProp	0.28	0.35
Pitman	-64.53	-170.78	71	56.7	-64.41	-64.11	-171.92	-170.32	5.0	Good	FaultProp	1.00	1.00
Raitt	-54.50	-119.50	146	85.8	-54.72	-54.06	-120.72	-118.44	5.0	Bad	GeoStruct	0.68	0.65
Saint Exupery	-62.24	-155.42	42	64.7	-62.40	-62.08	-155.83	-155.00	5.0	Bad	FaultProp	0.75	0.62
Tharp	-54.60	-131.00	462	83.5	-55.43	-53.76	-134.45	-127.96	5.8	Medium	FaultProp	0.64	0.28
Udintsev	-56.50	-142.40	325	78.8	-57.26	-55.66	-144.72	-140.33	5.6	Good	FaultProp	0.56	0.32
Vacquier	-53.10	-118.20	52	87.2	-53.14	-52.85	-118.70	-117.62	5.0	Medium	FaultProp	0.45	0.25
<u>South East Indian Ridge</u>													
Amsterdam	-36.60	78.60	108	67.0	-37.03	-36.30	78.17	79.22	5.0	Medium	GeoStruct	0.38	0.39
Balleny	-61.50	154.40	350	69.0	-63.21	-56.90	151.24	157.10	5.8	Bad	GeoStruct	0.33	0.12
Birubi	-49.30	127.40	148	74.4	-49.82	-47.83	126.87	128.03	5.0	Good	FaultProp	0.82	0.72
Boomerang	-37.40	78.20	35	67.2	-37.61	-37.25	77.94	78.47	5.0	Medium	FaultProp	0.61	0.54
Euroka	-49.20	126.10	134	74.6	-49.90	-47.94	125.57	126.78	5.0	Good	FaultProp	0.71	0.55
Geelvinck	-41.70	85.00	303	70.8	-42.58	-41.34	83.88	85.40	5.0	Bad	FaultProp	0.83	0.60
George V	-52.00	139.80	414	72.0	-56.97	-49.91	139.16	142.04	5.5	Bad	GeoStruct	0.58	0.36
Heemskerck	-50.01	115.58	101	70.3	-50.69	-48.79	115.41	116.90	5.0	Good	GeoStruct	0.81	0.63

Hillegom's Hole	-38.50	78.60	59	67.8	-38.85	-38.41	78.00	78.67	5.0	Medium	FaultProp	0.34	0.05
SEIR 100E	-47.80	99.80	129	74.7	-48.34	-46.69	98.97	100.93	5.0	Good	FaultProp	0.20	0.10
SEIR 107E	-48.80	106.50	130	75.3	-49.50	-47.99	105.90	107.21	5.0	Good	FaultProp	0.86	0.72
SEIR 120	-49.49	120.42	154	70.2	-50.16	-48.76	120.08	120.87	5.0	Bad	FaultProp	1.00	0.96
SEIR 121	-49.36	121.53	80	70.1	-49.76	-48.99	121.27	121.70	5.0	Bad	FaultProp	0.76	0.76
SEIR 122	-49.71	122.73	50	70.0	-50.00	-49.38	122.57	122.90	5.0	Bad	FaultProp	1.00	0.56
SEIR 88E	-42.00	88.30	65	71.7	-42.26	-41.54	87.92	88.94	5.0	Good	FaultProp	0.46	0.44
SEIR 96E (A)	-45.60	96.10	89	73.9	-46.04	-45.20	95.62	96.54	5.0	Good	FaultProp	0.44	0.41
SEIR 96E (B)	-46.50	95.90	40	74.0	-46.71	-46.21	95.77	96.36	5.0	Good	FaultProp	0.43	0.23
St Vincent	-54.50	144.12	58	66.5	-55.03	-53.82	142.11	145.20	5.0	Bad	FaultProp	0.50	0.37
Tasman	-57.80	147.70	625	70.1	-60.57	-54.01	146.35	150.34	5.2	Bad	GeoStruct	0.48	0.25
Ter Tholen	-33.20	77.80	89	65.2	-34.05	-32.79	77.03	78.54	5.0	Good	FaultProp	0.76	0.54
Vlamingh	-41.50	80.20	123	69.4	-42.00	-40.90	79.67	81.13	5.8	Good	FaultProp	0.31	0.15
Warringa	-49.41	123.38	87	70.0	-49.63	-48.80	123.33	123.96	5.0	Bad	FaultProp	1.00	0.47
Zeehaen	-50.23	114.07	62	70.4	-50.43	-49.30	113.83	114.80	5.0	Good	FaultProp	0.59	0.47
Zeewolf	-35.40	78.50	61	66.4	-35.60	-35.01	78.10	78.96	5.0	Good	FaultProp	0.78	0.60
<u>South Scotia Ridge</u>													
Shakleton	-59.11	-59.75	332	6.8	-60.95	-58.62	-62.44	-56.34	5.0	Good	FaultProp	0.89	0.77
<u>South West Indian Ridge</u>													
Andrew Bain	-50.10	30.00	706	14.6	-52.95	-47.00	27.62	32.28	5.2	Medium	FaultProp	0.83	0.65
Atlantis II	-32.80	57.00	201	14.6	-33.81	-31.73	56.73	57.40	5.0	Medium	GeoStruct	0.75	0.91
Bouvet	-54.20	1.90	201	13.8	-55.00	-53.41	0.44	3.27	5.0	Medium	FaultProp	0.45	0.22
Discovery II (A)	-43.40	41.60	124	14.8	-43.88	-42.42	41.25	41.95	5.0	Bad	FaultProp	0.71	0.63
Discovery II (B)	-41.90	42.50	216	14.8	-42.81	-40.88	42.11	42.93	5.0	Bad	FaultProp	0.75	0.75
Du Toit	-53.00	25.50	130	14.6	-53.77	-52.17	24.91	26.20	5.0	Good	FaultProp	0.51	0.34
Eric Simpson	-43.50	39.30	89	14.8	-43.88	-43.14	38.76	39.72	5.0	Bad	FaultProp	0.67	0.30
Gallieni	-36.64	52.32	114	12.3	-37.16	-36.09	52.16	52.46	5.0	Bad	FaultProp	0.63	0.54
Gauss	-35.00	54.12	59	12.2	-35.30	-34.71	54.08	54.19	5.0	Bad	FaultProp	0.38	0.10
Gazelle	-35.80	53.43	81	12.3	-36.18	-35.37	53.31	53.46	5.0	Bad	FaultProp	0.61	0.72
Indomed	-39.50	46.10	141	14.8	-40.30	-38.66	45.46	46.47	5.0	Bad	FaultProp	0.79	0.42
Islas Orcadas	-54.20	6.10	100	14.0	-54.62	-53.68	5.38	6.66	5.0	Bad	FaultProp	0.64	0.52
Marion	-46.60	33.70	109	14.7	-46.95	-45.51	33.27	34.26	5.0	Medium	FaultProp	0.63	0.57
Melville	-29.84	60.78	92	11.7	-30.77	-29.24	60.56	61.02	5.4	Medium	FaultProp	0.76	0.51
Novara	-31.43	58.41	45	11.9	-31.58	-31.09	58.34	58.52	5.0	Bad	FaultProp	0.69	0.66
Prince Edward	-45.40	35.10	146	14.7	-46.80	-45.16	34.53	35.40	5.0	Bad	FaultProp	0.44	0.19
Shaka	-53.50	9.30	199	14.1	-54.15	-52.56	8.03	10.23	5.4	Medium	FaultProp	0.35	0.26

*Bathymetry quality from Global Multi-Resolution Topography Data Synthesis (GMRT) is measured by visual inspection. *Good* if most major geological features can be identified clearly, *Medium* if only the ridge and transform fault can be clearly identified, otherwise *Bad* .

†Spatial segmentation type catagorized. *FaultProp* denotes that earthquake segmentation is not observed to be associated with large-scale geological structures, thus is infered due to variations of fault properties, *GeoStruct* denotes earthquake segmentation due to large-scale geological structures. *Undecided only* for Sovanco and Mabahiss due to being unable to assign a type.

§Creeping segment fraction. (*reloc)* denotes averaging by relocated events since 1990. (*1950)* denotes averaging by all events since 1950.

REFERENCES

Aderhold, K., and Abercrombie, R.E., 2016, The 2015 Mw 7.1 earthquake on the Charlie-Gibbs transform fault: Repeating earthquakes and multimodal slip on a slow oceanic transform: Geophysical Research Letters, v. 43, p. 6119–6128, doi:10.1002/2016GL068802.

Fox, C.G., Matsumoto, H., and Lau, T.-K.A., 2001, Monitoring Pacific Ocean seismicity from an autonomous hydrophone array: Journal of Geophysical Research: Solid Earth, v. 106, p. 4183–4206, doi:https://doi.org/10.1029/2000JB900404.

Hagberg, A.A., Schult, D.A., and Swart, P.J., 2008, Exploring Network Structure, Dynamics, and Function using NetworkX, *in* Varoquaux, G., Vaught, T., and Millman, J. eds., Proceedings of the 7th Python in Science Conference, Pasadena, CA USA, p. 11–15.

Howe, M., Ekström, G., and Nettles, M., 2019, Improving relative earthquake locations using surface-wave source corrections: Geophysical Journal International, v. 219, p. 297–312, doi:10.1093/gji/ggz291.

Johnson, S.G., 2020, The NLopt nonlinear-optimization package:, http://github.com/stevengj/nlopt.

McGuire, J.J., Collins, J.A., Gouédard, P., Roland, E., Lizarralde, D., Boettcher, M.S., Behn, M.D., and Hilst, R.D. van der, 2012, Variations in earthquake rupture properties along the Gofar transform fault, East Pacific Rise: Nature Geoscience, v. 5, p. 336–341, doi:10.1038/ngeo1454.

Nelder, J.A., and Mead, R., 1965, A Simplex Method for Function Minimization: The Computer Journal, v. 7, p. 308–313, doi:10.1093/comjnl/7.4.308.

Pan, J., Antolik, M., and Dziewonski, A.M., 2002, Locations of mid-oceanic earthquakes constrained by seafloor bathymetry: Journal of Geophysical Research: Solid Earth, v. 107, p. EPM 8-1-EPM 8-13, doi:10.1029/2001JB001588.

Pan, J., and Dziewonski, A.M., 2005, Comparison of mid-oceanic earthquake epicentral differences of travel time, centroid locations, and those determined by autonomous underwater hydrophone arrays: Journal of Geophysical Research: Solid Earth, v. 110, doi:https://doi.org/10.1029/2003JB002785.

Powell, M.J.D., 1994, A Direct Search Optimization Method That Models the Objective and Constraint Functions by Linear Interpolation, *in* Gomez, S. and Hennart, J.-P. eds., Advances in Optimization and Numerical Analysis, Dordrecht, Springer Netherlands, Mathematics and Its Applications, p. 51–67, doi:10.1007/978-94-015-8330-5_4.

PROJ contributors, 2020, PROJ coordinate transformation software library: Open Source Geospatial Foundation, https://proj.org/.

Shearer, P.M., 1997, Improving local earthquake locations using the L1 norm and waveform cross correlation: Application to the Whittier Narrows, California, aftershock sequence:

Journal of Geophysical Research: Solid Earth, v. 102, p. 8269–8283, doi:10.1029/96JB03228.

Virtanen, P. et al., 2020, SciPy 1.0: Fundamental Algorithms for Scientific Computing in Python: Nature Methods, v. 17, p. 261–272, doi:https://doi.org/10.1038/s41592-019-0686-2.

Waldhauser, F., and Ellsworth, W.L., 2000, A Double-Difference Earthquake Location Algorithm: Method and Application to the Northern Hayward Fault, California: Bulletin of the Seismological Society of America, v. 90, p. 1353–1368, doi:10.1785/0120000006.

Wells, D.L., and Coppersmith, K.J., 1994, New empirical relationships among magnitude, rupture length, rupture width, rupture area, and surface displacement: Bulletin of the Seismological Society of America, v. 84, p. 974–1002, https://pubs.geoscienceworld.org/ssa/bssa/article-abstract/84/4/974/119792/New-empirical-relationships-among-magnitude (accessed July 2020).

Wolfson-Schwehr, M., Boettcher, M.S., McGuire, J.J., and Collins, J.A., 2014, The relationship between seismicity and fault structure on the Discovery transform fault, East Pacific Rise: Geochemistry, Geophysics, Geosystems, v. 15, p. 3698–3712, doi:10.1002/2014GC005445.

Wright, M., 1996, Direct search methods: Once scorned, now respectable: Numerical analysis: Proceedings of the 1995 Dundee Biennial Conference in Numerical Analysis, p. 191–208, https://nyuscholars.nyu.edu/en/publications/direct-search-methods-once-scorned-now-respectable (accessed July 2020).